Journal of Sound and Vibration (2001) **241**(4), 567–586
doi:10.1006/jsvi.2000.3144, available online at http://www.idealibrary.com on IDEAL®

CHATTER PREDICTION OF END MILLING IN A VERTICAL MACHINING CENTER

S. K. Kim

Graduate School of Automotive Engineering, Kookmin University, 861-1, *Chongnung-dong, Songbuk-gu, Seoul* 136-702, *South Korea. E-mail: rhett@mailvib.snu.ac.kr*

AND

S.-Y. Lee

School of Mechanical Engineering, Kunsan National University, 68, *Miryong-dong, Kunsan, Chonbuk* 573-701, *South Korea*

(*Received* 18 *February* 2000, *and in final form* 13 *June* 2000)

The development of a high-speed and high-precision vertical machining center had been executed as a national project in Korea. In the machining center, the phenomenon of chatter vibration was an important factor, and should be examined for developing it by a relevant way. In a high-speed and high-precision vertical machining center, in order to observe and predict the chatter vibration, firstly, modal testing was performed to obtain modal parameters of the system. Secondly, in order to predict the cutting forces for end-milling process under various cutting conditions, a simplified model was presented. Finally, the chatter prediction for the vertical machining center was formulated as linear differential–difference equations, and verified by the cutting tests. The method in this work will provide an engineer who designs a machining center with a tool to predict the chatter phenomenon.

1. INTRODUCTION

In machining operation, the chatter may often limit the quantities of large feed and workpiece–tool engagement. The chatter phenomenon is known to be generated by a transient vibration existing between the tool and workpiece, and results in the pattern of irregularities on the surface of workpiece [1]. The machine tool and the workpiece have a structural system with very complicated dynamic characteristics, and in the simulation of the behavior of a machine tool, numerous factors are required like a lot of parameters of the cutting dynamics. Also, the self-induced chatter is generated by a lot of cutting operations involving the overlapping cuts. Although the system might be basically stable, the forced vibration resulting from the machining of the wavy surface from a previous stroke or the rotation of workpiece and the tool could have an effect on the previous vibration, and amplify it hugely.

In a high-speed and high-precision vertical machining center, the chatter vibration is readily generated by the unbalanced masses of the rotating parts and the variations of cutting forces. In order to predict the chatter characteristics of the vertical machining center, it is necessary to identify the structural dynamic characteristics of the machine and the cutting dynamics. In the work of Sridhar *et al.* [2], a general formulation of milling process equation in machining center was shown.

0022-460X/01/140567 + 20 $35.00/0

A coefficient of constant peripheral cutting resistance and the constants of the cutting force ratio were used in machining with helical end mills [3]. Altintas *et al.* [4] and Minis *et al.* [5] presented a constant specific cutting pressure and the cutting force ratio in milling with straight end mills. Tarng [6] expressed the specific cutting pressure with a tangential force and the ratio of the radial force to the tangential force as an exponential function of the averaging chip thickness per revolution. Smith *et al.* [7] introduced a constant cutting stiffness and considered the radial force to be proportional to the tangential force.

In the last several decades, a number of studies and researches have been performed on the chatter vibration of the machine tool. Also, many works have been conducted on the prediction of the chatter phenomenon in milling. However, no one has studied the chatter prediction of end milling. Kline *et al.* [8] just showed the way to predict the cutting force in end milling. The purpose of this work is to represent how to predict the chatter in end milling in a vertical machining center using a simplified model and the experiments. The simplified model consists of two degrees of freedom, a direction of feed and the orthogonal one to the feed.

A simplified model is built to predict the chatter phenomenon in the vertical machining center. This model is based on Kline *et al.* [8] considering chip load, cutting geometry, and the relationship between the cutting forces and the chip load. Specific cutting constants of the model are obtained from averaging forces measured by the cutting tests. The interactions between the dynamic characteristics and the cutting dynamics of the vertical machining center make the primary and secondary feedback loops, and are used in the equations of motion of the system to predict the chatter vibration [2, 4, 5, 7]. The chatter prediction is formulated as linear differential–difference equations, and is verified by experiments.

2. STRUCTURAL DYNAMICS OF THE VERTICAL MACHINING CENTER

The structural dynamics in the vertical machining center is assumed to be two orthogonal modes, x–y axes, since a table with a workpiece has a much larger stiffness, compared with spindle–tool system (x–y axes). This assumption is applied to ordinary milling machines. In Figure 1, each axis defined for simplified model and end milling in a vertical machining center is shown. A simplified model for chatter prediction in the vertical machining center system is shown in Figure 2.

The equations of motion for the structural dynamics in a vertical machining center are given as

$$\begin{aligned} m_1\ddot{x} + b_1\dot{x} + k_1 x &= F_x(t), \\ m_2\ddot{y} + b_2\dot{y} + k_2 y &= F_y(t). \end{aligned} \tag{1}$$

Parameters m_1, b_1 and k_1 are mass, damping and stiffness in the x direction, respectively, and the x-axis is the feeding direction. Also, parameters m_2, b_2 and k_2 are the mass, damping and stiffness in the y direction orthogonal to the feeding direction, respectively. Each parameter is an equivalent value, and modal analyses in the x and y directions are conducted. The data are obtained from using LMS Cada-x software package. The reason to assume that each viscous damping is linear like stiffness is for the damping value to be generally known to be small in the spindle–tool system. The measured and calculated data for each parameter will be shown in detail in Section 6. The equations of motion will be solved, after $F_x(t)$ and $F_y(t)$ are defined from cutting dynamics in the next section.

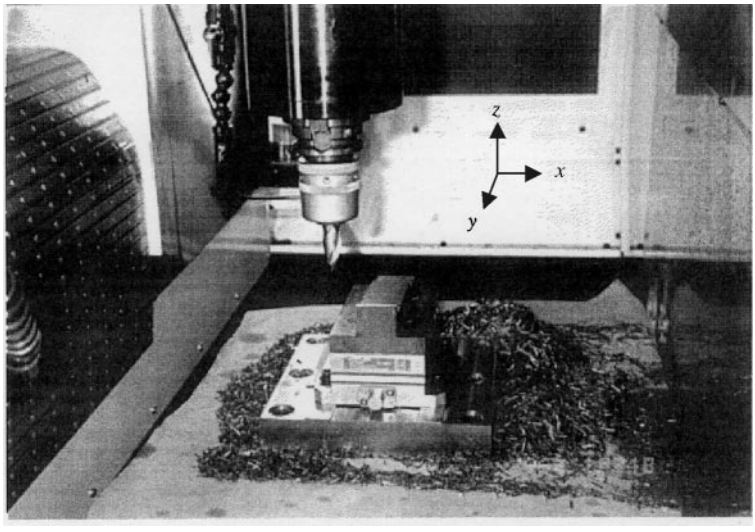

Figure 1. End milling in a vertical machining center.

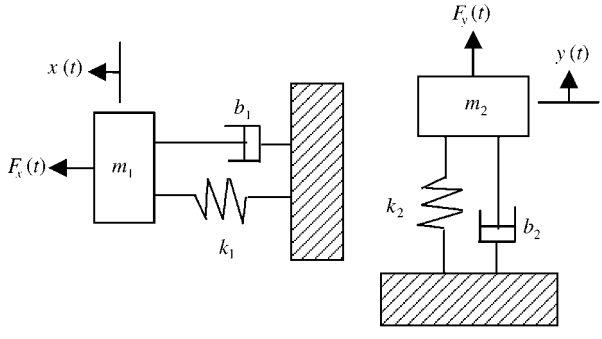

Figure 2. Schematic of a simplified model for structural dynamics in a vertical machining center.

3. THE CUTTING DYNAMICS OF THE VERTICAL MACHINING CENTER

A basic element for predicting the cutting force is how to define the chip load on the tool. The most general expression for chip thickness is given as

$$t_c = f \sin \beta, \tag{2}$$

where t_c, f and β are the instantaneous chip thickness, feed rate per tooth and angular position of a flute of tool under cutting, respectively, as shown in Figure 3.

Total sum of the chip load of the end-mill at an arbitrary instant is obtained from adding to each chip load on the shallow circular disks, and those disks are divided along the axis of tool. Generally, in milling machining the ways to cut are down and up. In this work, only the down cutting is considered, since the down cutting is of a more general type in the vertical machining center. The cutting forces are composed of the tangential cutting force which is proportional to the chip load and the radial cutting force which is proportional to

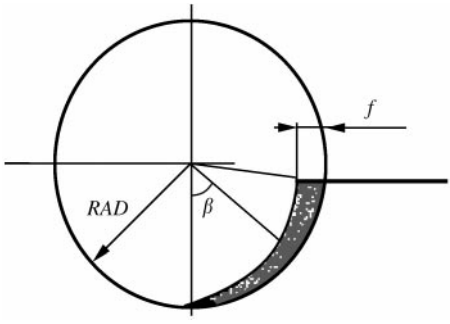

Figure 3. Schematic of feed and angular position in end milling in a vertical machining center.

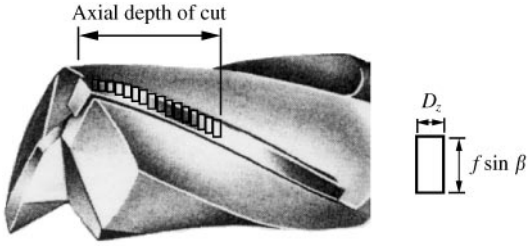

Figure 4. Schematic of end-mill and cutting geometry.

the tangential cutting force as

$$\Delta F_{\tan} = K_{T0} D_z t_c, \tag{3}$$

$$\Delta F_{rad} = K_R \Delta F_{\tan}, \tag{4}$$

where $\Delta F_{\tan}$, ΔF_{rad}, D_z and t_c are the tangential force on the current small disk, the radial force on the small disk, the small cutting width and the chip load in equation (2), respectively. K_{T0} and K_R are constants from equation (8) and experiments [8], and it is found that the specific cutting constant K_{T0} is varied by the chip thickness. In Figure 4, end-mill and cutting geometry are shown.

The tangential force, $\Delta F_{\tan}$ is rewritten as

$$\Delta F_{\tan} = K_T D_z f \sin \beta. \tag{5}$$

The specific cutting constant K_T in equation (5) is also varied by the cutting conditions, which are the feed, the radial depth of cut and the axial depth of cut. When tool radius, number of the flutes and helix angle are RAD, N_f and α_{hx}, respectively, the instant angular position $\beta(i, k, t)$ is given from cutting geometry in the down cutting as

$$\beta(i, k, t) = -\theta(t) + \frac{2\pi}{N_f}(k-1) + \left(i - \frac{1}{2}\right) D_z \times \frac{\tan \alpha_{hx}}{RAD}, \tag{6}$$

where i, t, $\theta(t)$ and k are the address number of small axial circular disk, the operating time, the rotating angle of the lowest part of the first flute at time t, and the number of flutes, respectively. Among the calculated $\beta(i, k, t)$ values from equation (6), only the values within the cutting range affect the cutting forces. The tangential and radial directions are divided

into x and y components of global co-ordinates, and the total sums in each directional cutting force are like

$$F_x(t) = \sum_{i=1}^{N_z} \sum_{k=1}^{N_f} \{ -\Delta F_{rad}(i,k,t) \sin[\beta(i,k,t)] + \Delta F_{\tan}(i,k,t) \cos[\beta(i,k,t)]\},$$
$$F_y(t) = \sum_{i=1}^{N_z} \sum_{k=1}^{N_f} \{\Delta F_{rad}(i,k,t) \cos[\beta(i,k,t)] + \Delta F_{\tan}(i,k,t) \sin[\beta(i,k,t)]\}. \quad (7)$$

If the average cutting forces are defined in the cutting condition where the feed, the radial and axial depths of cut for a given tool are fixed, a pair of K_R and K_T can be calculated from the only one test, since the average cutting forces are functions of K_R and K_T.

The parameters K_R and K_T are functions of the feed, the radial and axial depths of cut, and they are assumed to be calculated using the least-squares method by changing values of the feed, the radial and axial depths of cut as

$$K_T = a_0 + a_1 RD + a_2 AD + a_3 f + a_4 RDAD + a_5 fRD + a_6 fAD + a_7 RD^2 + a_8 AD^2 + a_9 f^2,$$
$$K_R = b_0 + b_1 RD + b_2 AD + b_3 f + b_4 RDAD + b_5 fRD + b_6 fAD + b_7 RD^2 + b_8 AD^2 + b_9 f^2, \quad (8)$$

where a_0–a_9 and b_0–b_9 are constant coefficients, and RD, AD and f are the radial depth of cut, the axial depth of cut and the feed, respectively.

4. DYNAMIC CUTTING STATE

In dynamic cutting state, a deflection behavior in the system results from the cutting force. Then, this behavior affects the depth of cut, and results in the variation of the depth of cut [2]. A block diagram of total chatter loop is shown in Figure 5.

The deflection in the feed direction, $x(t)$ increases the depth of cut, and the deflection in the y direction, $y(t)$ decreases the depth of cut. Firstly, the case without regeneration is considered. The equation for the primary feedback is given as

$$u_P(i,k,t) = x(t) \sin[\beta(i,k,t)] - y(t) \cos[\beta(i,k,t)], \quad (9)$$

where plus sign indicates that the depth of the cut increases and minus sign indicates that it decreases in relative vibration.

The current chip thickness is affected by the remaining chip amount at a previous flute, and this is the regeneration. The remaining amount at the $(k-1)$th flute increases the chip thickness of the kth flute, when the kth flute comes to the position after T s. This

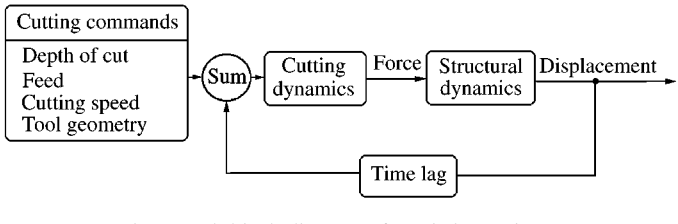

Figure 5. A block diagram of total chatter loop.

phenomenon is the regeneration feedback, and can be written as

$$u_R(i,k,t) = -\mu x(t-T)\sin[\beta(i,k,t)] + \mu y(t-T)\cos[\beta(i,k,t)], \tag{10}$$

where $T = 60/(nN_f)$, n and μ are the time lag between two flutes and the spindle speed whose unit is revolutions per minute and an overlap factor respectively.

Total deviation of the chip thickness is the sum of the primary and regenerative deviations, and the instantaneous chip thickness is the sum of the nominal chip thickness and the total deviation like

$$\begin{aligned} u(i,k,t) &= f\sin\beta + u_P(i,k,t) + u_R(i,k,t) \\ &= f\sin\beta + \{x(t)\sin\beta - y(t)\cos\beta\} + \{\mu x(t-T)\sin\beta + \mu y(t-T)\cos\beta\}, \\ u(i,k,t) &= \{\sin[\beta(i,k,t)]\ \cos[\beta(i,k,t)]\} \begin{Bmatrix} x(t) - \mu x(t-T) + f \\ -y(t) + \mu y(t-T) \end{Bmatrix}. \end{aligned} \tag{11}$$

The cutting forces are rewritten as

$$\begin{aligned} F_x(t) &= \sum_{i=1}^{N_z}\sum_{k=1}^{N_f} \{ -\Delta F_{rad}\sin[\beta(i,k,t)] + \Delta F_{\tan}\cos[\beta(i,k,t)]\} \\ &= \sum_{i=1}^{N_z}\sum_{k=1}^{N_f} \{ -K_R K_T D_z u(i,k,t)\sin\beta + K_T D_z u(i,k,t)\cos\beta\} \\ &= \sum_{i=1}^{N_z}\sum_{k=1}^{N_f} \{ -K_R K_T D_z \sin[\beta(i,k,t)] + K_T D_z \cos[\beta(i,k,t)]\} u(i,k,t), \\ F_y(t) &= \sum_{i=1}^{N_z}\sum_{k=1}^{N_f} \{\Delta F_{rad}\cos[\beta(i,k,t)] + \Delta F_{\tan}\sin[\beta(i,k,t)]\} \\ &= \sum_{i=1}^{N_z}\sum_{k=1}^{N_f} \{K_R K_T D_z u(i,k,t)\cos\beta + K_T D_z u(i,k,t)\sin\beta\} \\ &= \sum_{i=1}^{N_z}\sum_{k=1}^{N_f} \{K_R K_T D_z \cos[\beta(i,k,t)] + K_T D_z \sin[\beta(i,k,t)]\} u(i,k,t) \end{aligned} \tag{12, 13}$$

and

$$\begin{aligned} \begin{Bmatrix} F_x(t) \\ F_y(t) \end{Bmatrix} &= K_T D_z \begin{bmatrix} \sum_{i=1}^{N_z}\sum_{k=1}^{N_f} [-K_R\sin\beta + \cos\beta] \\ \sum_{i=1}^{N_z}\sum_{k=1}^{N_f} [K_R\cos\beta + \sin\beta] \end{bmatrix} \{\sin\beta\ \ \cos\beta\} \begin{Bmatrix} x(t) - \mu x(t-T) + f \\ -y(t) + \mu y(t-T) \end{Bmatrix} \\ &= K_T D_z \sum_{i=1}^{N_z}\sum_{k=1}^{N_f} \begin{bmatrix} -K_R\sin^2\beta + \cos\beta\sin\beta & -K_R\cos\beta\sin\beta + \cos^2\beta \\ K_R\cos\beta\sin\beta + \sin^2\beta & K_R\cos^2\beta + \cos\beta\sin\beta \end{bmatrix} \\ &\quad \times \begin{Bmatrix} x(t) - \mu x(t-T) + f \\ -y(t) + \mu y(t-T) \end{Bmatrix}. \end{aligned} \tag{14}$$

Equation (14) is substituted into equation (1). Finally, the equations of motion of the chatter vibration in the vertical machining center are derived.

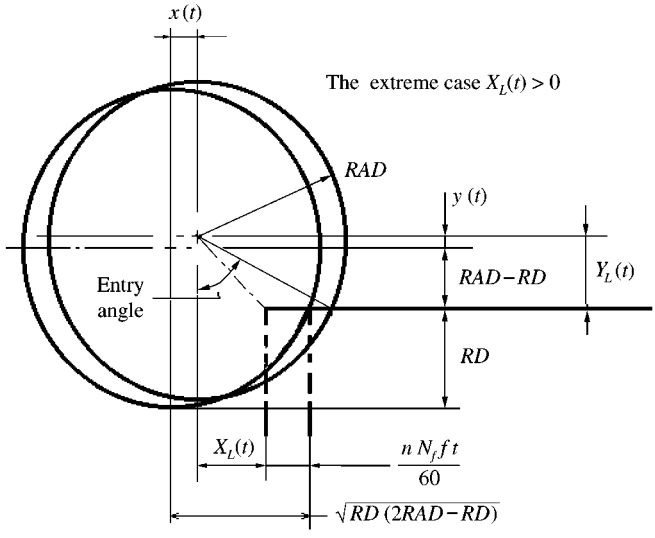

Figure 6. Schematic of the tool entry and exit.

The next step is to analyze chatter vibration in the range where the cutting lengths are from 0 to the tool diameter, and divide the range into a very large integer. The time interval between the flutes is multiples of the integer of the small time. The velocity and displacement of the next time step are determined from the finite difference or Newmark method, and the cutting force is calculated from substituting them into equation (14). The relative virtual positions in the x and y directions of the tool center to workpiece when moving with the time are given as

$$X_L(t) = \sqrt{RD(2RAD - RD)} - \frac{nN_f ft}{60} - x(t), \tag{15}$$

$$Y_L(t) = RAD - RD + y(t), \tag{16}$$

where $\sqrt{RD(2RAD - RD)}$ is the distance in the x direction from the tool center to workpiece when cutting is started, $(nN_f ft)/60 - x(t)$ is the traveling of the workpiece, $x(t)$ is the relative vibration, and *RAD-RD* is the distance in the y direction from the tool center to workpiece.

A schematic drawing is shown in Figure 6.

In $\alpha_{ex} \leqslant$ cutting range $\leqslant \alpha_{en}$, the angles of the tool entry and exit are written as

$$\alpha_{en}(t) = \cos^{-1}\left(\frac{RAD - RD + y(t)}{RAD}\right),$$
$$\alpha_{ex}(t) = 0 \quad \text{or} \quad \sin^{-1}\left(\frac{X_L(t)}{RAD}\right). \tag{17}$$

5. EXPERIMENTAL DETERMINATION OF THE SPECIFIC CUTTING CONSTANTS

The purpose of the experiments is to measure the cutting forces under the various cutting conditions in end-milling, and the measured values are used to obtain the specific cutting constants as described in equation (8). A block diagram for the total procedure of the experiments and the calculation of the specific cutting constants is shown in Figure 7.

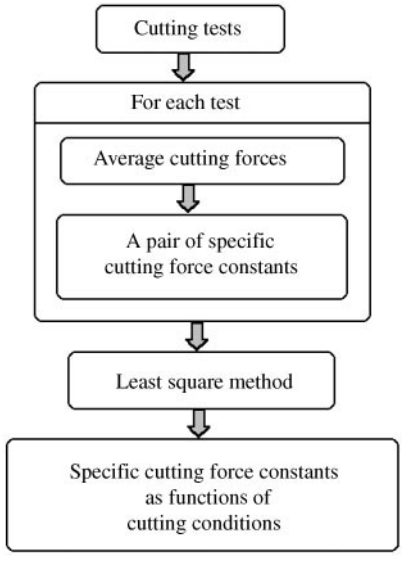

Figure 7. Schematic of a block diagram for the experiments and the calculation of the specific cutting constants.

TABLE 1

Cutting conditions for tests

End mill	Diameter: 16 mm, 2 edges
Radial depth of cut (mm)	2·0, 3·0, 4·0, 5·0, 6·0
Axial depth of cut (mm)	10·0, 13·0, 16·0
Feed (FEED, mm/min)	80·0, 100·0, 120·0
Spindle speed (r.p.m.)	400·0, 600·0

TABLE 2

Conditions for simulations

Total number of tests	90
Increment of angle of cutter (deg)	1·0
Number of axial disk elements of cutter	10·0, 13·0, 16·0
Angles at which cutter exits cutting (deg)	0·0
Helix angle of cutter (deg)	30·0
Rake angle (ω, deg)	0·0

The specific cutting constants were determined experimentally from the cutting tests of the vertical machining center. Those tests were under various cutting conditions, and the constants of equation (8) were calculated with a program built by the least-squares method. The vertical machining center used in this paper was of type ACE-V35, which was being manufactured by Daewoo Heavy Industries and the tool dynamometer KISTLER-9257B was used to measure the cutting forces. The cutting conditions for the tests are given in Table 1. For the simulations, FORTRAN commercial program was used under the conditions listed in Table 2, and for each axial depth of cut, average cutting forces in the x and y directions obtained from tests are shown in Tables 3 (a–c).

The coefficients of the specific cutting constants were obtained as in Table 4.

TABLE 3

Average cutting forces in the x and y directions from tests

Radial depth of cut (mm)	Feed (mm/min)	Spindle speed (r.p.m.)	Average *x*-cutting force (N)	Average *y*-cutting force (N)
(a) *Axial depth of cut* = 10 mm				
2.0	80·0	400·0	290·56	360·07
		600·0	205·89	264·58
	100·0	400·0	318·37	386·07
		600·0	224·61	288·05
	120·0	400·0	468·54	489·34
		600·0	249·38	304·62
3.0	80·0	400·0	344·25	494·69
		600·0	231·21	346·58
	100·0	400·0	390·31	543·20
		600·0	260·49	395·01
	120·0	400·0	455·37	606·84
		600·0	300·92	442·71
4.0	80·0	400·0	365·22	608·94
		600·0	251·90	448·09
	100·0	400·0	429·72	688·94
		600·0	280·78	509·30
	120·0	400·0	488·22	764·59
		600·0	324·62	568·45
5.0	80·0	400·0	375·02	724·38
		600·0	256·93	553·84
	100·0	400·0	443·41	804·04
		600·0	280·88	626·98
	120·0	400·0	524·99	955·52
		600·0	338·20	717·69
6.0	80·0	400·0	366·21	877·01
		600·0	243·31	648·80
	100·0	400·0	438·98	964·97
		600·0	277·43	732·35
	120·0	400·0	520·96	1067·12
		600·0	332·39	848·28
(b) *Axial depth of cut* = 13 mm				
2.0	80·0	400·0	342·35	413·39
		600·0	247·89	326·53
	100·0	400·0	394·69	462·56
		600·0	255·71	341·36
	120·0	400·0	436·47	509·84
		600·0	293·94	374·85
3.0	80·0	400·0	409·53	581·78
		600·0	272·35	417·61
	100·0	400·0	474·09	635·17
		600·0	312·91	501·75
	120·0	400·0	544·68	721·07
		600·0	357·79	541·50

TABLE 3

(*Continued*)

Radial depth of cut (mm)	Feed (mm/min)	Spindle speed (r.p.m.)	Average *x*-cutting force (N)	Average *y*-cutting force (N)
	80·0	400·0	436·74	733·95
		600·0	288·95	521·70
4.0	100·0	400·0	527·40	820·41
		600·0	341·91	658·11
	120·0	400·0	615·94	946·51
		600·0	394·25	709·40
	80·0	400·0	452·20	883·57
		600·0	296·08	634·37
5.0	100·0	400·0	550·58	1027·88
		600·0	347·87	819·21
	120·0	400·0	643·25	1138·53
		600·0	405·69	882·80
	80·0	400·0	466·07	1069·63
		600·0	287·62	747·19
6.0	100·0	400·0	565·90	1227·80
		600·0	333·78	973·95
	120·0	400·0	674·78	1400·60
		600·0	398·21	1045·99
(c) *Axial depth of cut* = 16 mm				
	80·0	400·0	344·73	428·77
		600·0	277·18	383·82
2.0	100·0	400·0	439·87	545·17
		600·0	303·14	417·43
	120·0	400·0	485·17	598·10
		600·0	355·32	451·19
	80·0	400·0	448·0	687·17
		600·0	315·69	517·40
3.0	100·0	400·0	524·97	745·82
		600·0	350·14	557·11
	120·0	400·0	584·75	801·55
		600·0	422·90	618·03
	80·0	400·0	495·90	885·44
		600·0	323·77	647·33
4.0	100·0	400·0	596·23	960·89
		600·0	381·77	715·81
	120·0	400·0	682·40	1068·17
		600·0	453·45	809·14
	80·0	400·0	521·85	1076·65
		600·0	335·08	804·32
5.0	100·0	400·0	641·44	1187·25
		600·0	400·25	880·59
	120·0	400·0	734·10	1323·59
		600·0	475·22	1009·70
	80·0	400·0	519·49	1281·61
		600·0	323·77	937·38
6.0	100·0	400·0	634·51	1383·63
		600·0	391·85	1033·50
	120·0	400·0	758·84	1589·07
		600·0	472·55	1201·96

TABLE 4

Coefficients of the specific cutting force by simulations

a_i	a_0	$0{\cdot}107 \times 10^{11}$
	a_1	$-0{\cdot}114 \times 10^{13}$
	a_2	$-0{\cdot}232 \times 10^{12}$
	a_3	$-0{\cdot}282 \times 10^{14}$
	a_4	$0{\cdot}212 \times 10^{14}$
	a_5	$0{\cdot}611 \times 10^{15}$
	a_6	$-0{\cdot}192 \times 10^{15}$
	a_7	$0{\cdot}683 \times 10^{14}$
	a_8	$0{\cdot}268 \times 10^{13}$
	a_9	$0{\cdot}890 \times 10^{17}$
b_i	b_0	0·538
	b_1	−33·575
	b_2	2·247
	b_3	−331·263
	b_4	$-0{\cdot}112 \times 10^{4}$
	b_5	$-0{\cdot}102 \times 10^{6}$
	b_6	$-0{\cdot}357 \times 10^{5}$
	b_7	$0{\cdot}409 \times 10^{4}$
	b_8	$0{\cdot}355 \times 10^{3}$
	b_9	$-0{\cdot}208 \times 10^{6}$

TABLE 5

The equivalent parameters by LMS

	Equivalent mass (kg)	Equivalent damping (kg/s)	Equivalent stiffness (N/m)
x direction	44·84	4368	$0{\cdot}1361 \times 10^{9}$
y direction	36·36	3387	$0{\cdot}1320 \times 10^{9}$

6. RESULTS OF NUMERICAL ANALYSIS

Using the built program, the dynamic displacements under the various cutting conditions were calculated. Also, modal testing was performed to pick out the x and y directional equivalent parameters of the used vertical machining center as equation (1). HP-workstation with LMS modal software (single-degree-of-freedom method) was used to obtain them. In Table 5, the equivalent parameters by LMS are shown.

In simulations, four different dynamic analyses were executed. The first is that the axial depth of cut = 16 mm, main spindle speed = 600 r.p.m., the feed rate = 120 mm/min, and the radial depths of cut are varied as 2, 4, 6 and 8 mm. The results of the first analysis are shown in Table 6. It is found that by increasing the radial depth of cut, the dynamic displacements in the x and y directions increase. In Figure 8, the results for the radial depth of cut = 2 mm are shown. The results that the radial depths of cut are 4 and 6 mm are shown in Figures 9 and 10. In Figure 8, although the dynamic displacements increase with

TABLE 6

The results of the dynamic analysis for axial depth of cut = 16 mm, *spindle speed* = 600 r.p.m. *and feed rate* = 120 mm/min (*maximum displacement only*)

Displacement (μm)	Radial depth of cut			
	2·0 mm	4·0 mm	6·0 mm	8·0 mm
x	10·95	35·23	94·51	472·0
y	16·13	62·99	172·7	795·7

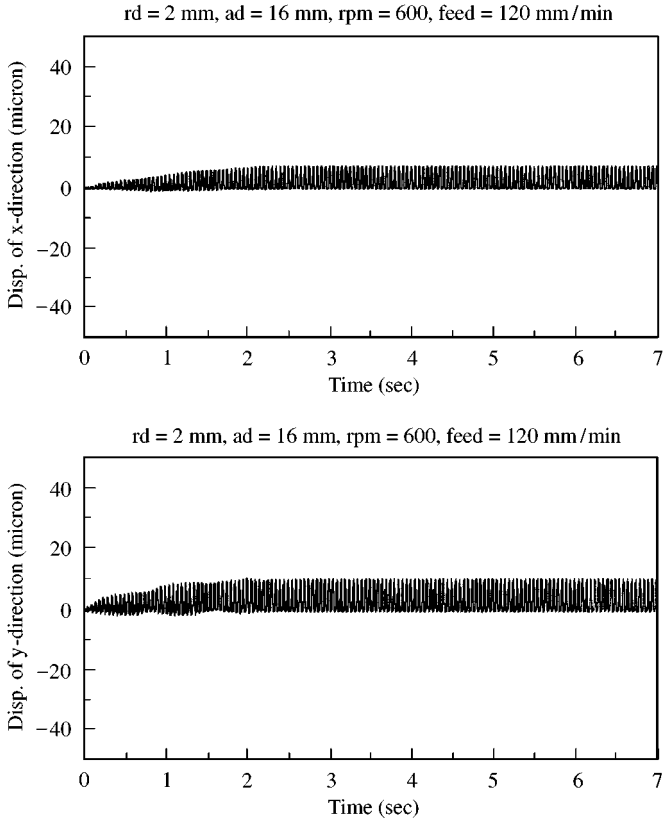

Figure 8. Dynamic displacement analysis of a vertical machining center for radial depth of cut = 2 mm, axial depth of cut = 16 mm, spindle speed = 600 r.p.m. and feed = 120 mm/min.

the time, after a constant time the amplitude of vibration becomes stable. In case the radial depths of cut are larger than 4 mm, dynamic displacements increase hugely after a transition time.

The second analysis is that the radial depth of cut = 6 mm, the spindle speed = 600 r.p.m., the feed rate = 120 mm/min, and the axial depths of cut are varied as 10, 13 and

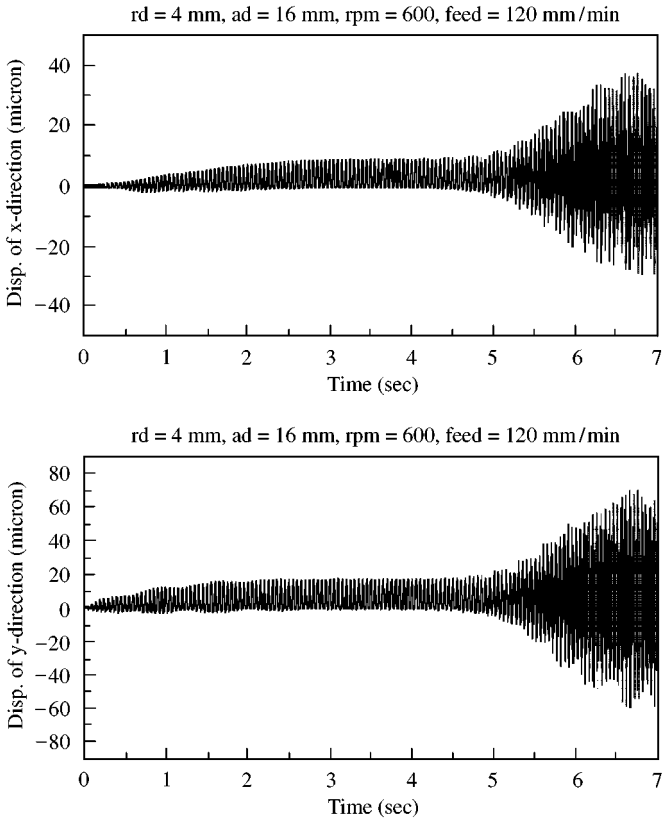

Figure 9. Dynamic displacement analysis of a vertical machining center for radial depth of cut = 4 mm, axial depth of cut = 16 mm, spindle speed = 600 r.p.m. and feed = 120 mm/min.

16 mm. The results are given in Table 7, and it is found that as the axial depth of cut increases, the dynamic displacements in the x and y directions increase. In Figure 11, the results for the axial depth of cut = 10 mm, and after going by a constant time the amplitude of vibration becomes stable. In case the axial depths of cut are larger than 13 mm as in Figure 12, the dynamic displacements increase hugely after a transition time.

The third is that the axial depth of cut = 16 mm, the main spindle speed = 400 r.p.m., the feed rate = 120 mm/min, and the radial depths of cut are changed as 2, 4, 6, 8 and 10 mm. The results are shown in Table 8. It is found that by increasing the radial depth of cut, the dynamic displacements in the x and y directions increase, similarly to Table 6. In Figure 13, the results for the radial depth of cut = 2 mm are shown. The other results that the radial depths of cut are 6, 8 and 10 mm are shown in Figures 14, 15 and 16 respectively. In Figures 13 and 14, although the dynamic displacements increase with the time, after a constant time the amplitude of vibration becomes stable like in previous simulations. In Figure 15 where the radial depth of cut is 8 mm, the amplitude of vibration is large, but it cannot be said that chatter is generated. In Figure 12 where the radial depth of cut is 10 mm, dynamic displacements also increase hugely after a transition time as in previous results.

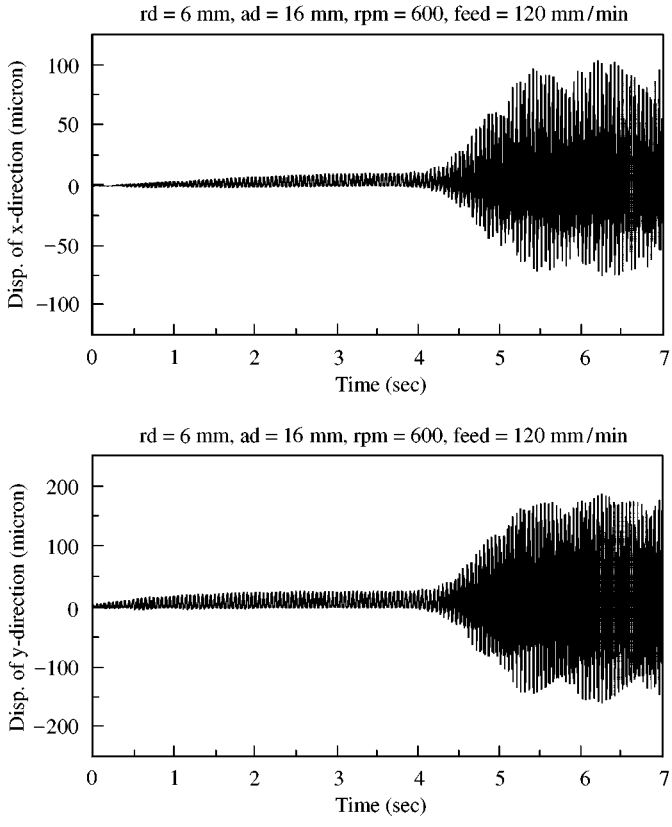

Figure 10. Dynamic displacement analysis of a vertical machining center for radial depth of cut = 6 mm, axial depth of cut = 16 mm, spindle speed = 600 r.p.m. and feed = 120 mm/min.

TABLE 7

The results of the dynamic analysis for radial depth of cut = 6 mm, *spindle speed* = 600 r.p.m. *and feed rate* = 120 mm/min (*maximum displacement only*)

Displacement (μm)	Axial depth of cut		
	10·0 mm	13·0 mm	16·0 mm
x	8·79	29·21	94·51
y	24·03	50·72	172·7

The fourth analysis is that the radial depth of cut = 6 mm, the spindle speed = 600 r.p.m., the feed rate = 120 mm/min., and the axial depths of cut are varied as 10, 13, 16 and 19 mm. The results of the final analysis are given in Table 9. It is found that as the axial depth of cut increases, the *x* and *y* dynamic displacements increase as in previous simulations. In Figure 17, the results for the axial depth of cut = 13 mm are shown. After

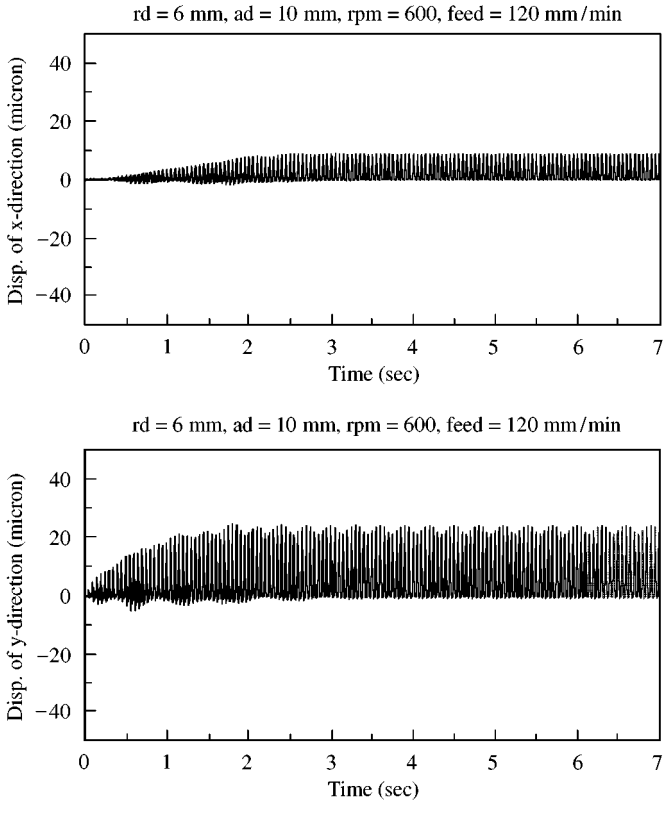

Figure 11. Dynamic displacement analysis of a vertical machining center for radial depth of cut = 6 mm, axial depth of cut = 10 mm, spindle speed = 600 r.p.m. and feed = 120 mm/min.

a constant time the amplitude of vibration also becomes stable. In Figure 18 where the axial depth of cut is 19 mm, the dynamic displacements also increase hugely after a transition time.

7. CONCLUSIONS

In machine tool, it is very important to predict the chatter vibration since the chatter affects the surface of a workpiece severely and the quality of the product becomes the worst. Numerous studies and researches for the chatter phenomenon have been performed in the last several decades. Especially, a number of works on the chatter have been done in a high-speed and high-precision machine tool. The purpose of this work is to present how to predict the chatter prediction of end milling in a vertical machining center using a simplified model.

A high-speed and high-precision vertical machining center has been developed as a national project in Korea in the last couple of years. Some results for the chatter of the vertical machining center are as follows. Firstly, a simplified model was presented, and this model has two degrees of freedom. The model was built, based on the chip load, the cutting geometry, and the relationship between the cutting forces and the chip load. Secondly, to

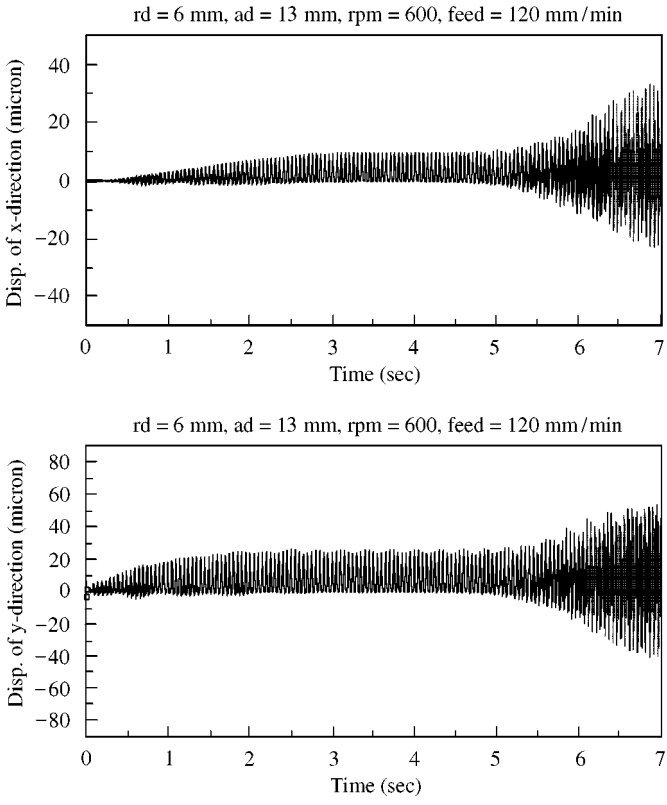

Figure 12. Dynamic displacement analysis of a vertical machining center for radial depth of cut = 6 mm, axial depth of cut = 13 mm, spindle speed = 600 r.p.m. and feed = 120 mm/min.

TABLE 8

The results of the dynamic analysis for axial depth of cut = 16 mm, *spindle speed* = 400 r.p.m. *and feed rate* = 120 mm/min (*maximum displacement only*)

Displacement (μm)	Radial depth of cut			
	2·0 mm	6·0 mm	8·0 mm	10·0 mm
x	10·18	15·60	19·11	519·0
y	12·49	33·28	50·47	853·9

measure the cutting forces of end-milling process, the cutting tests were performed for various cutting conditions. All the tests were executed in the machining center manufactured by Daewoo Heavy Industries. Thirdly, the modal testing was performed to obtain equivalent modal parameters of the vertical machining center by using LMS commercial program package. Fourthly, the cutting forces measured from cutting tests were applied to the model to calculate the specific cutting constants used in the model. Finally,

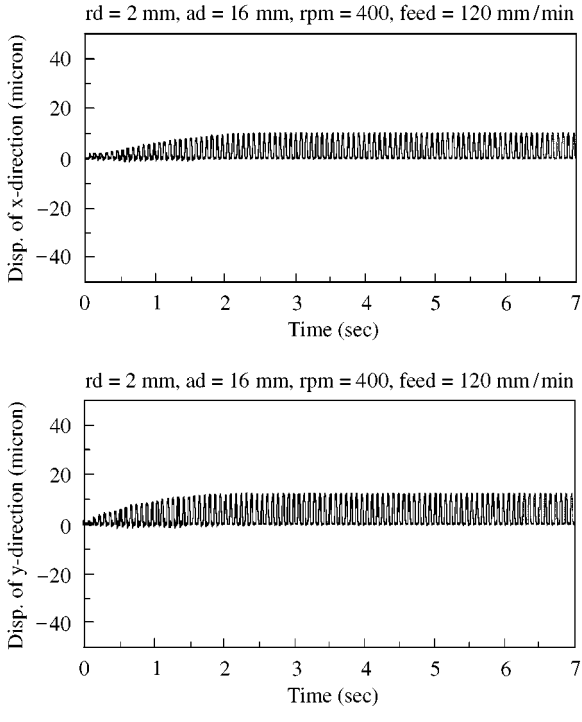

Figure 13. Dynamic displacement analysis of a vertical machining center for radial depth of cut = 2 mm, axial depth of cut = 16 mm, spindle speed = 400 r.p.m. and feed = 120 mm/min.

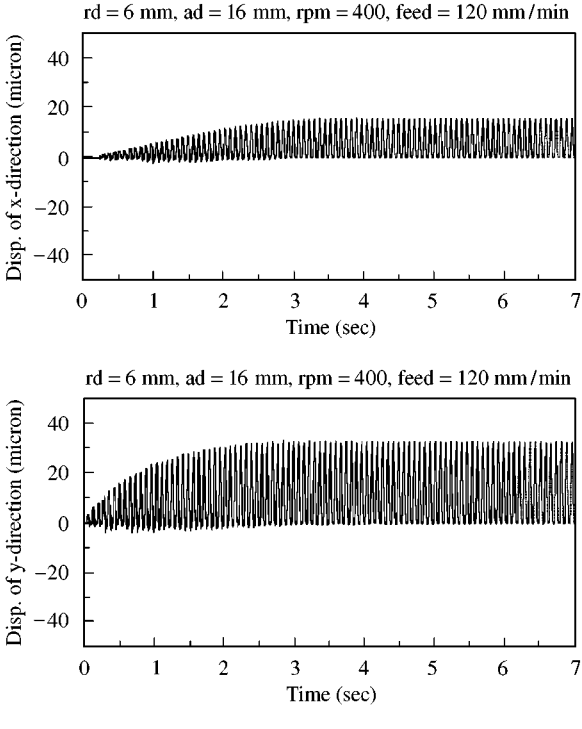

Figure 14. Dynamic displacement analysis of a vertical machining center for radial depth of cut = 6 mm, axial depth of cut = 16 mm, spindle speed = 400 r.p.m. and feed = 120 mm/min.

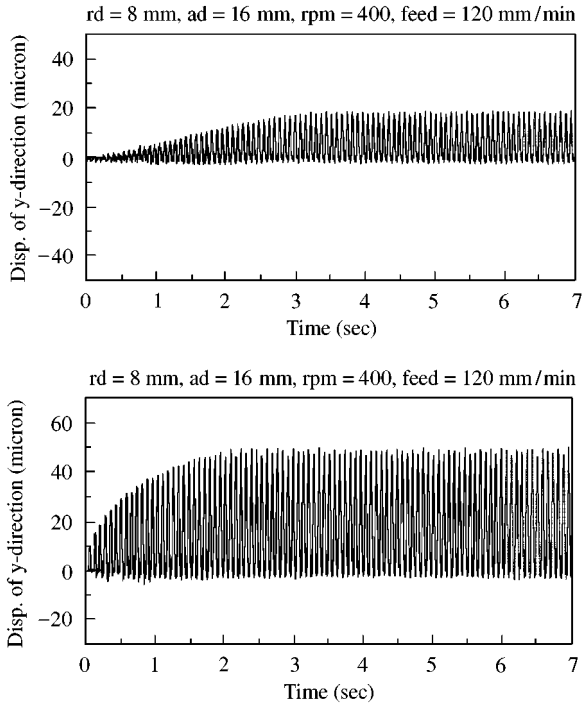

Figure 15. Dynamic displacement analysis of a vertical machining center for radial depth of cut = 8 mm, axial depth of cut = 16 mm, spindle speed = 400 r.p.m. and feed = 120 mm/min.

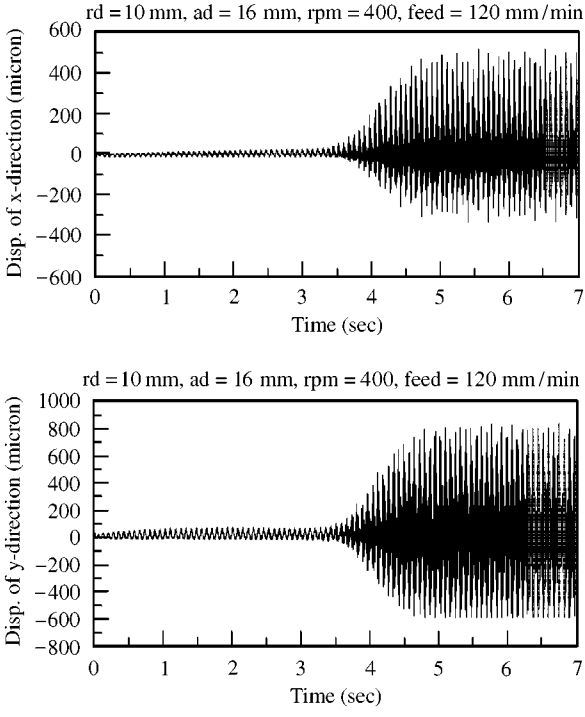

Figure 16. Dynamic displacement analysis of a vertical machining center for radial depth of cut = 10 mm, axial depth of cut = 16 mm, spindle speed = 400 r.p.m. and feed = 120 mm/min.

TABLE 9

The results of the dynamic analysis for radial depth of cut = 6 mm, *spindle speed* = 400 r.p.m. *and feed rate* = 120 mm/min (*maximum displacement only*)

Displacement (μm)	Axial depth of cut			
	10·0 mm	13·0 mm	16·0 mm	19·0 mm
x	13·22	14·92	15·60	16·23
y	31·49	33·36	33·28	34·90

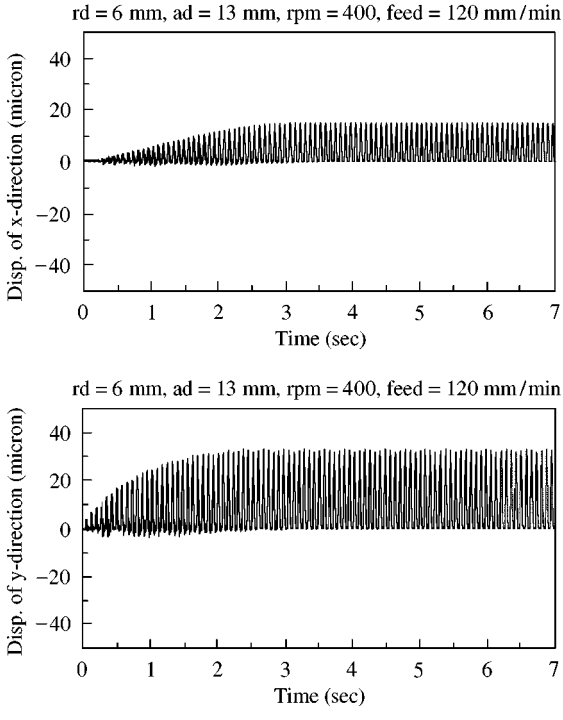

Figure 17. Dynamic displacement analysis of a vertical machining center for radial depth of cut = 6 mm, axial depth of cut = 13 mm, spindle speed = 400 r.p.m. and feed = 120 mm/min.

the program to analyze the dynamic displacements under the specific cutting condition was written. The dynamic displacements for the various cutting conditions were given in time domain, and were verified by the experiments. It was found that the interactions between the dynamic characteristics and the cutting dynamics of the vertical machining center made the primary and the secondary feedback loops through the simulations.

By the method presented in this study, the chatter phenomenon was analyzed clearly for a high-speed and high-precision vertical machining center. Especially, from the simulations for the changes of the cutting conditions, it was predicted when the chatter was generated in time domain. The method was used as a tool to analyze the chatter phenomenon in end milling of machining center in Korea, and will be used in end milling in any kind of a machining center.

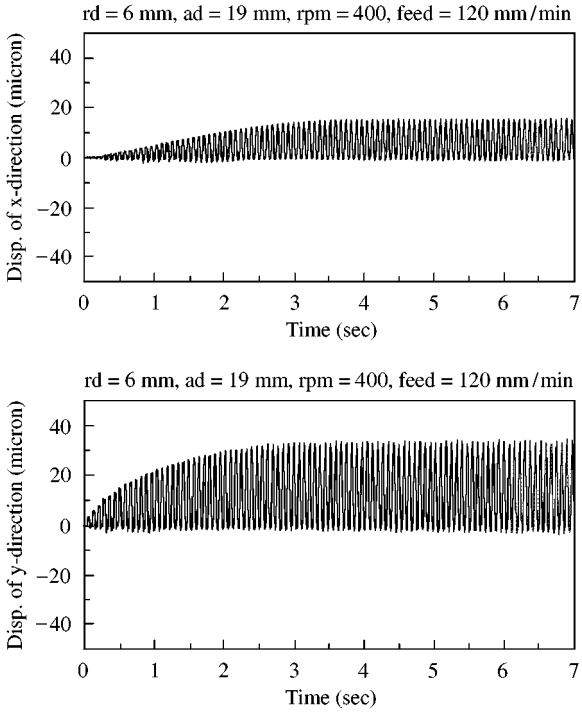

Figure 18. Dynamic displacement analysis of a vertical machining center for radial depth of cut = 6 mm, axial depth of cut = 19 mm, spindle speed = 400 r.p.m. and feed = 120 mm/min.

ACKNOWLEDGMENTS

The authors wish to express gratitude to Daewoo Heavy Industries Ltd. for their support, both financial and intellectual. Without their support, this research would not have been possible. Also, this work was supported by the Brain Korea 21 Project.

REFERENCES

1. G. BOOTHROYD 1981 *Fundamentals of Metal Machining and Machine Tools*. New York: McGraw-Hill International Book Co.
2. R. SRIDHAR, R. E. HOHN and G. W. LONG 1968 *Transactions of ASME Journal of Engineering for Industry* **90**, 317–324. A general formulation of the milling process equation.
3. A. BER, J. ROTBERG and S. ZOMBACH 1988 *Annals of the CIRP* **37**, 37–40. A method for cutting force evaluation of end mills.
4. Y. ALTINTAS and P. K. GHAN 1992 *International Journal of Machine Tool Design and Research*. **32**, 329–347. In-process detection and suppression of chatter in milling.
5. I. MINIS, R. YANUSHEVSKY and A. TEMBO 1990 *Annals of the CIRP* **39**, 459–462. Analysis of linear and nonlinear chatter in milling.
6. Y. S. TARNG, C. I. CHENG and J. Y. KAO 1995 *International Journal of Machine Tool Design and Research* **35**, 939–950. Modeling of three-dimensional numerically controlled end milling operations.
7. S. SMITH and J. TLUSTY 1993 *Annals of the CIRP* **42**, 463–466. Efficient simulation programs for chatter in milling.
8. W. A. KLINE, R. E. DEVOR and J. R. LINDBERG 1982 *International Journal of Machine Tool Design and Research* **22**, 7–22. The prediction of cutting forces in end milling with application to cornering cuts.